A unified model for dynamic and static stress triggering of aftershocks, antishocks, remote seismicity, creep events, and multisegmented rupture

Christophe Voisin, Fabrice Cotton, Sara Di Carli

A unified model for dynamic and static stress triggering of aftershocks, antishocks, remote seismicity, creep events, and multisegmented rupture

Christophe Voisin, Fabrice Cotton, and Sara Di Carli

Laboratoire de Géophysique Interne et Tectonophysique, CNRS, Observatoire des Sciences de l'Univers de Grenoble, Université Joseph Fourier, Grenoble, France

Received 10 November 2003; revised 31 March 2004; accepted 6 May 2004; published 16 June 2004.

[1] Aftershocks have been thought to be triggered by static stress transfer. The 1992 Landers and 1999 Hector Mine, California, earthquakes have demonstrated the possibility of remote triggering of seismicity, highlighting the role of dynamic seismic waves. Static stress changes and transient deformations have different timescales. The mechanisms by which they trigger earthquakes are thought to be different, leading to an unwieldy vision of aftershock triggering. We propose a model that encompasses both static and dynamic triggering of aftershocks and antishocks as well as the occurrence of stable slip (creep events) or multisegmented rupture. The framework of this model is based on the stability/instability transition of faults. We propose that dynamic and static stress triggering pertain to the same physical process. We study the effect of the complete Coulomb failure function. We demonstrate the possibility of the triggering of seismicity by a dynamic stress pulse in a stress shadow zone characterized by a negative static stress field. The limited time efficiency of dynamic triggering shown by the data is explained by the model. We suggest that dynamic waves trigger only the most unstable faults associated with a relatively short characteristic time, while the static stress field triggers also faults that are stable, associated with a larger characteristic time. *INDEX TERMS:* 7209 Seismology: Earthquake dynamics and mechanics; 7260 Seismology: Theory and modeling; 7230 Seismology: Seismicity and seismotectonics; *KEYWORDS:* seismicity triggering, complete Coulomb failure function, slip-dependent friction

Citation: Voisin, C., F. Cotton, and S. Di Carli (2004), A unified model for dynamic and static stress triggering of aftershocks, antishocks, remote seismicity, creep events, and multisegmented rupture, *J. Geophys. Res.*, *109*, B06304, doi:10.1029/2003JB002886.

1. Introduction

[2] It has been proposed that aftershocks are triggered by shear stress increase (*Smith and Van de Lindt* [1969] and *Hamilton* [1972] for the 1968 Borrego Mountain, California, earthquake and *Rybicki* [1973], *Yamashina* [1978], and *Das and Scholz* [1981] for the 1979 Homestead Valley, California, earthquake). Since then, the theory of Coulomb stress change has been developed to combine both shear stress and normal stress changes into a single variable named Coulomb failure stress [*Kadinsky-Cade and Willemann*, 1982; *Stein and Lisowski*, 1983]. This theory has been applied with success to the case of large earthquakes around the world (see *Harris* [1998] for a review). A positive correlation is observed between the number of aftershocks and regions of calculated Coulomb stress increase (stress trigger). Reciprocally, a deficiency of aftershocks is observed where a Coulomb stress decrease (stress shadow) is computed. The 1992 Landers, California, earthquake has raised the possibility of long-distance triggering [*Hill et al.*, 1993; *Anderson et al.*, 1994]. *Bodin and Gomberg* [1994] and *Gomberg and Bodin* [1994] have studied the triggering of the M_s 5.4 Little Skull Mountain 22 hours after the Landers main shock. They related the occurrence of this large remote aftershock to the dynamic strain tensor. Major earthquakes are now found to trigger remote seismicity: the 1999 Hector Mine, California, earthquake [*Gomberg et al.*, 2001; *Glowacka et al.*, 2002] and the 1999 Izmit, Turkey, earthquake [*Brodsky et al.*, 2000]. *Kilb et al.* [2000, 2002] and *Gomberg et al.* [2003] have demonstrated that the seismicity rate change correlates better with the dynamic stress field than with the static stress change. Their results also suggest that dynamic triggering is efficient at close distances from the main shock as well as at long distances. This is in good agreement with previous studies that demonstrated the influence of the dynamic stress field in the propagation of a multisegmented rupture [*Harris et al.*, 1991; *Harris and Day*, 1993; *Kame and Yamashita*, 1997; *Kase and Kuge*, 1998, 2001; *Voisin et al.*, 2000; *Antonioli et al.*, 2003], suggesting that the underlying physics are the same in both phenomena.

[3] However, dynamic triggering is having difficulty with another observation, stress shadows [*Reasenberg and Simpson*, 1992; *Simpson and Reasenberg*, 1994; *Harris*

0148-0227/04/2003JB002886$09.00

and Simpson, 1996, 1998]. Stress shadows occur when an earthquake has reduced the Coulomb failure stress on appropriately oriented nearby faults. They are associated with a seismicity rate decrease [*Parsons et al.*, 1999; *Stein*, 1999] followed by a time-dependent recovery. Because dynamic stresses oscillate, they are positive everywhere at some time. Therefore the dynamic stresses cast no stress shadow, and by consequence they are not consistent with observations of seismicity rate decrease [*Stein*, 1999]. *Marone* [2000] even suggested that to document a shaking-induced increase in seismicity rate in a stress shadow would be one way to prove the role of dynamic triggering. We will show in this study that stress shadows are compatible with dynamic triggering.

[4] Another difficulty appears when comparing dynamic and static stress triggering. Dynamic stress waves have a shorter duration than static stress changes. How to explain their ability to trigger seismicity? Can we expect long triggering delays [e.g., *Gomberg et al.*, 1998; *Kilb et al.*, 2000] from dynamic stresses? There have already been several attempts to consider both static and dynamic triggering. *Gomberg et al.* [1998] and *Belardinelli et al.* [2003] have investigated the triggering by dynamic and static stress changes, using rate and state formulations for the frictional behavior of the faults. They show that static and dynamic changes have different net effects on a fault obeying rate and state friction. A static stress change is able to advance or delay an induced instability depending on its sign, while a dynamic stress pulse is only able to promote a nearly instantaneous failure, provided its amplitude is positive and large enough with respect to the direct effect of friction [*Belardinelli et al.*, 2003]. On the contrary, *Gomberg et al.* [1997, 1998] and *Kilb et al.* [2000] all expect a long time delay for dynamic triggering. More recently, *Kilb* [2003] pointed out the strong correlation between the peak dynamic Coulomb stress change induced by the 1992 Landers earthquake and the hypocenter of the 1999 Hector Mine earthquake. If the dynamic triggering is the only mechanism, this would imply a time delay of 9 years. *Cotton and Coutant* [1997] proved that dynamic and static Coulomb failure patterns are different for unilateral ruptures. However, it was difficult to infer in the near field which of the two mechanisms, static or dynamic, was relevant to aftershock triggering. Using a slip-dependent friction law [e.g., *Ohnaka*, 1996], *Voisin et al.* [2000] have investigated the relative weight of static and dynamic stress changes in the triggering of the 1980 Irpinia earthquake sequence. Although it was not possible to rule out the possibility of static triggering, or the possibility of dynamic plus static triggering of the second event, they concluded that in such a case of near-field triggering the dynamic pulse emitted by the main shock was strong enough to trigger the second event with a time delay of nearly 20 s. *Voisin* [2001, 2002] focused more specifically on the dynamic triggering of a fault under slip-dependent friction. It was shown that the occurrence of triggering depends on the balance between the loading terms and the intrinsic mechanics of the fault, governed by the friction law. The amplitude and frequency of the incident wave were found to exert a clock advance effect [*Voisin*, 2001]. *Voisin* [2002] extended the results to the case of nonlinear slip-dependent friction. It was shown that two qualitative behaviors were possible for the faults. Some faults may exhibit a threshold in frequency for triggering, while some other faults may exhibit a threshold in amplitude. For fault mechanics under slip-dependent friction [*Dascalu et al.*, 2000; *Voisin et al.*, 2002] it was shown that the faults with a threshold in frequency are intrinsically unstable, while the faults with a threshold in amplitude are stable. Because of the nonlinearity of the friction law it was demonstrated that under a sufficient loading (dynamic or static), the faults could experience a transition from stability to instability. In the model proposed by *Voisin* [2002], both dynamic and static loadings affect the occurrence of triggering. This suggests that they should be considered as one and only one perturbation, in a complete Coulomb failure function [*Kilb et al.*, 2000; *Voisin et al.*, 2000], and not independently as done in previous work.

[5] The goal of this paper is therefore to study the effect of the complete Coulomb failure function (CFF) on the triggering of slip-dependent faults. In this paper, we will consider idealized complete Coulomb failure functions of three types. Since the static stress field at remote distance is negligible, the far-field CFF will be represented by a simple sine wave [*Voisin*, 2001, 2002]. In the near field we will consider two CFFs: one for stress triggers, formed of a dynamic pulse followed by a positive static stress step, and one for stress shadows, formed of a dynamic pulse followed by a negative static stress step. As will be shown, it is crucial to consider both dynamic and static loadings and not only the peak of the dynamic CFF, especially to understand what happens in stress shadows.

[6] For each of the three types of complete Coulomb failure function we will indicate what faults are triggered and what is the triggering delay, that is, the time lag between the loading and the eventual rupture. The triggering delay is related to a characteristic time included in a friction law, either rate and state [*Gomberg et al.*, 1997, 1998; *Belardinelli et al.*, 1999, 2003; *Perfettini et al.*, 2003a, 2003b] or slip-dependent [*Voisin et al.*, 2000; *Voisin*, 2001, 2002].

[7] Using these simulations, we will address the following questions:

[8] (1) Is it possible to trigger an antishock, that is, an earthquake in a stress shadow [*Stein*, 1999]?

[9] (2) What are the parameters (external loading properties and intrinsic fault properties) that control the triggering threshold? How do these parameters interact to trigger or not trigger an earthquake?

[10] (3) What parameters control the time delay between the stress loading and the eventual triggering?

[11] The outline of the paper is as follows: Section 2 presents the model and the numerical values used to perform the simulations. Section 3 focuses on the triggering of seismicity in a stress shadow. Section 4 presents the numerical simulations and the resulting implications for triggering. Section 5 compares the numerical results with the real data of the 1992 Landers, California, and the 1999 Hector Mine, California, aftershock sequences. Finally, section 6 discusses the implications of the model on the regional seismic hazard changes after a major event.

2. Model

2.1. Finite Fault

[12] The model is described by *Voisin* [2001, 2002]. We consider a two-dimensional antiplane finite fault of length

L = 10 km, a typical value for a fault segment. The shear wave velocity is c = 3000 m/s, and the density of the medium is ρ = 3000 kg/m^3. The normal stress S_N is assumed to correspond to a depth of 5 km.

[13] In the case of an infinite homogeneous fault under linear slip-dependent friction, *Campillo and Ionescu* [1997] established that the time of evolution of the initiation process is mainly related to the friction parameters

$$t \approx \frac{1}{c\alpha} \ln \frac{\pi D_c}{2l(W_0 + W_1/c)}, \quad (1)$$

where c is the S wave celerity, α corresponds to the slope of friction divided by the rigidity modulus, D_c is the critical slip, and W_0, W_1, and l are parameters of the perturbation. This result was extended by *Ionescu and Campillo* [1999] to show that the initiation duration is strongly dependent on the slope of friction and on the size of the slipping patch. Using a finite difference scheme, they carried out experiments with initiation duration of about 100 s. Finally, *Dascalu et al.* [2000] defined a nondimensional parameter β that governs the intrinsic mechanics of the fault. They described the existence of a universal constant β_0 that depends only on the geometry of the fault (or of the fault system). β_0 separates a domain of stability ($\beta < \beta_0$) from a domain of instability ($\beta > \beta_0$). They showed that in the case of a finite slipping patch, the characteristic time of evolution is related to the growth rate of slip instability λ,

$$t \approx \frac{a}{c\lambda} \ln \frac{c\lambda D_c/A + \sqrt{(c\lambda D_c/A)^2 - (\lambda c W_0)^2 + (aW_1)^2}}{\lambda c W_0 + aW_1}, \quad (2)$$

where a is the length of the slipping patch, A is a function of β, and c, W_0, and W_1 have the same significance as above. The most interesting consequence is that when β tends to β_0, the growth rate of instability λ tends to zero, and, reciprocally, the characteristic time of evolution tends to infinity. In other words, this simple model of friction allows for a wide range of time delay [*Dascalu et al.*, 2000].

2.2. Friction Law

[14] A nonlinear friction law with varying weakening rate is used [*Ionescu and Campillo*, 1999]. The friction law is described by $\tau_s = \mu_s S_N$, $\tau_d = \mu_d S_N$, D_c, and a parameter p of range [0,1], which are the static friction, the dynamic friction, the critical slip, and a modulation factor, respectively [*Voisin*, 2002]. The friction law is nonlinear with respect to the displacement u and is given by

$$\mu(u) = \mu_s - \frac{\mu_s - \mu_d}{D_c} \left[u - (1-p) \frac{D_c}{2\pi} \sin\left(\frac{2\pi u}{D_c}\right) \right]. \quad (3)$$

Here μ_s and μ_d are chosen to impose a stress drop of 11.5 MPa. The friction decreases from τ_s to τ_d with the ongoing slip. The weakening rate is α(u),

$$\alpha(u) = -\frac{S_N}{G} \mu'(u), \quad (4)$$

where $\mu'(u)$ is the derivative of friction with respect to displacement, G is the rigidity modulus, and S_N is the normal stress. Following *Dascalu et al.* [2000] and *Voisin* [2002], we define $\beta(u)$ as

$$\beta(u) = \alpha(u) \frac{L}{2}. \quad (5)$$

This nondimensional parameter controls the intrinsic fault mechanics. *Dascalu et al.* [2000] have performed a static stability analysis and found the first eigenvalue β_0 that determines the range of instability for the dynamic problem. The fault behavior is governed by the relative magnitude of β and β_0. In the case $\beta < \beta_0$ the fault is stable, that is, no slip or slip velocity instability can develop on the fault; this is the nucleation phase. In the case $\beta > \beta_0$ the fault is unstable; this is the initiation phase [*Campillo and Ionescu*, 1997]. As the slip reaches D_c, the friction stabilizes at the residual dynamic level; this is the rupture propagation phase (Figure 1). Throughout this paper, we will consider homoge-

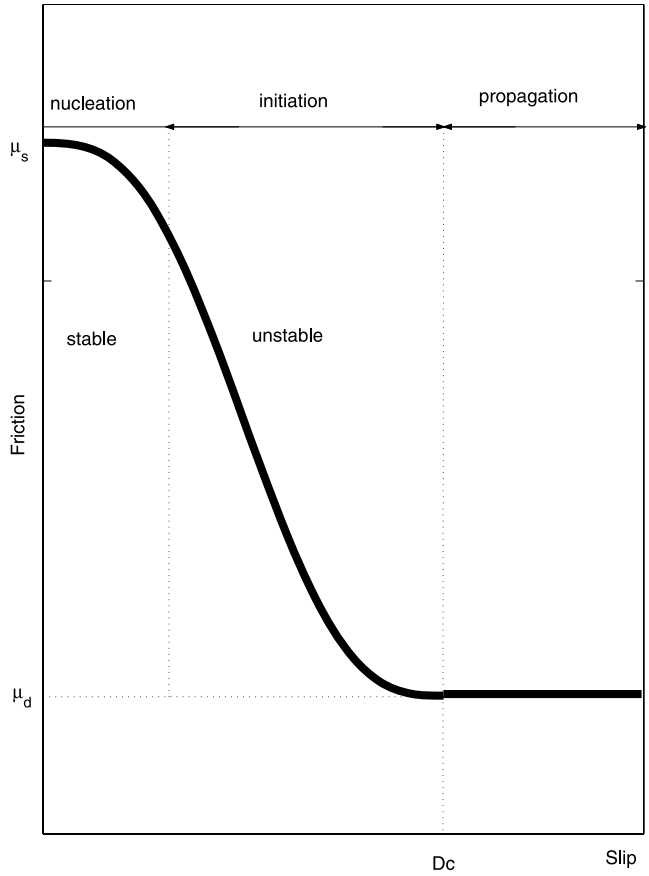

Figure 1. Nonlinear slip-dependent friction law. The shear stress degrades as the slip increases from zero to the critical slip D_c. During the phase of nucleation the slope of the friction (given through β) is too low to promote the development of a slip instability; this phase is stable, and its characteristic time is of the order of years to centuries. On the contrary, the initiation phase is unstable; the slope of the friction law is large enough to sustain the development of slip instability ($\beta > \beta_0$). Its characteristic time ranges between 1 s to 1 hour. As the slip reaches D_c, this is the end of the initiation phase and the beginning of the rupture propagation on the fault.

neous friction properties over the fault. In the case of a heterogeneous fault, L could stand for the length of the fault, or any shorter characteristic length, typical of the roughness of the fault surfaces or of its width. *Campillo et al.* [2001] and *Voisin et al.* [2002] have shown that the heterogeneous fault can be represented by an equivalent homogeneous fault, with an enhanced stability. By consequence, the stability condition must be given relative to a size. A fault can be at the same time stable at the overall scale and unstable at the local scale. Therefore the finite homogeneous fault with slip weakening friction used in the present study must be understood as representing the global behavior of a heterogeneous fault.

2.3. State of Stress

[15] The state of stress on the fault and in the medium equals the static friction level. This static friction level can be considered as a first threshold to be overcome for an eventual rupture. This allows us to focus only on the effect of the perturbation and to compare the results with previous studies [*Voisin*, 2001, 2002].

2.4. External Loadings

[16] Figure 2 presents the three external loadings considered in this study. As discussed in section 1, we consider an idealized complete Coulomb failure function. In the far field the static stress loading is negligible, and the CFF is restricted to its dynamic component, idealized as a simple sine pulse without any static stress field. In the near field we examine the stress trigger CFF and the stress shadow CFF. The stress trigger CFF is composed of the same dynamic pulse followed by a positive static stress field. The stress shadow CFF is composed of the same dynamic pulse followed this time by a negative static stress field.

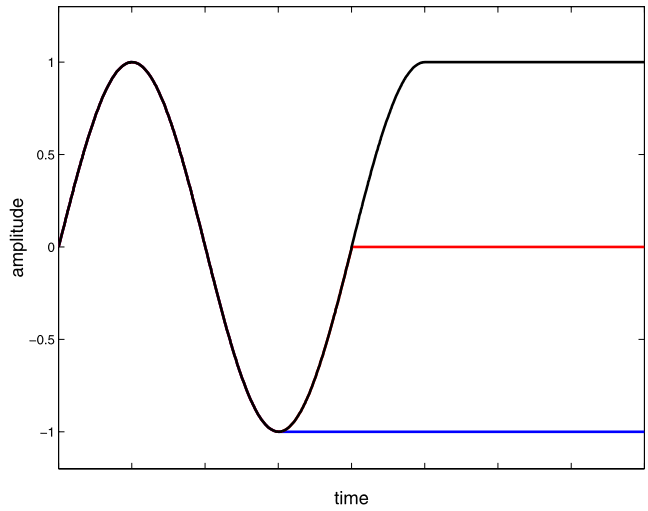

Figure 2. Three complete Coulomb failure functions (CFF) considered in this study. They all share the same dynamic evolution: a stress pulse of unit amplitude followed by a different static stress field. The static stress field (black curve) has a unit positive amplitude (stress trigger CFF). The null amplitude static stress field (red curve) has a far-field CFF. The unit negative amplitude static stress field (blue curve) has a stress shadow CFF.

3. Seismicity Triggering in Stress Shadows

[17] In this section we demonstrate the possibility of the triggering of seismicity by a dynamic stress pulse in a stress shadow zone characterized by a negative static stress field. To this end we consider the CFF presented in Figure 2 for the stress shadow case. It is composed of a positive dynamic pulse followed by a negative static stress field.

[18] Figure 3 presents the space-time evolution of the stress field on and around the fault. This stress field is the net result of the summation of the incident stress loading and of the secondary stress field generated by the slip on the fault. At time $t = 0$ s the external loading is at the tip of the fault. The positive pulse is clearly visible and is followed by the negative static stress field. At time $t = 1$ s the external loading has propagated throughout the medium and has reached the fault. A first stress concentration, linked to the initiation process on the fault, is visible at the fault tip. At $t = 2$ s the loading is propagating through the fault. The initiation process enhanced by the positive pulse is inhibited by the negative static stress loading. At $t = 3.4$ s the stress wave has reached the opposite tip of the fault: The second stress concentration is visible. One can see also a zone of stress decrease in the vicinity of this fault tip; this is the nucleation zone. This zone is growing laterally as the shear stress decreases down to the residual friction level. At time $t = 5.87$ s the nucleation process is at work, in spite of the incident negative static stress field. The shear stress reaches the residual, dynamic friction level at time $t = 9$ s (not shown). At this time the rupture front propagates along the fault until it reaches the fault tips. At time $t = 13.3$ s one can see that the release of the shear stress along the fault has fed the shear stress concentrations at the fault tips. The numerical result presented above would not have been observed if we were to consider only the negative static stress field. The triggering of an antishock is possible only if we consider the dynamic and static parts of the Coulomb failure function, that is, the complete CFF.

4. Triggering Threshold and Temporal Aspects of Triggering Under Slip-Dependent Friction

4.1. Effect of the Shape of the Coulomb Failure Function

[19] In this section we determine the factors controlling the occurrence of triggering. For the sake of simplicity we restrict ourselves to a linear friction case. This also allows for a comparison with the results of *Voisin* [2001] obtained for a dynamic stress pulse only (to simulate long-distance triggering).

[20] We consider the three loadings, presented in Figure 2. The frequency of the stress pulse is set to $f = 1$ Hz. With the numerical values of the parameters of the model, there is a condition of instability given by $\beta > \beta_0$, which in terms of D_c, turns to

$$D_c \leq 1.9 \text{ m}.$$

That is, as long as D_c is lower than 1.9 m, the fault is unstable and can be triggered. Above this limit the fault is stable and cannot be triggered. Only stable slip may occur

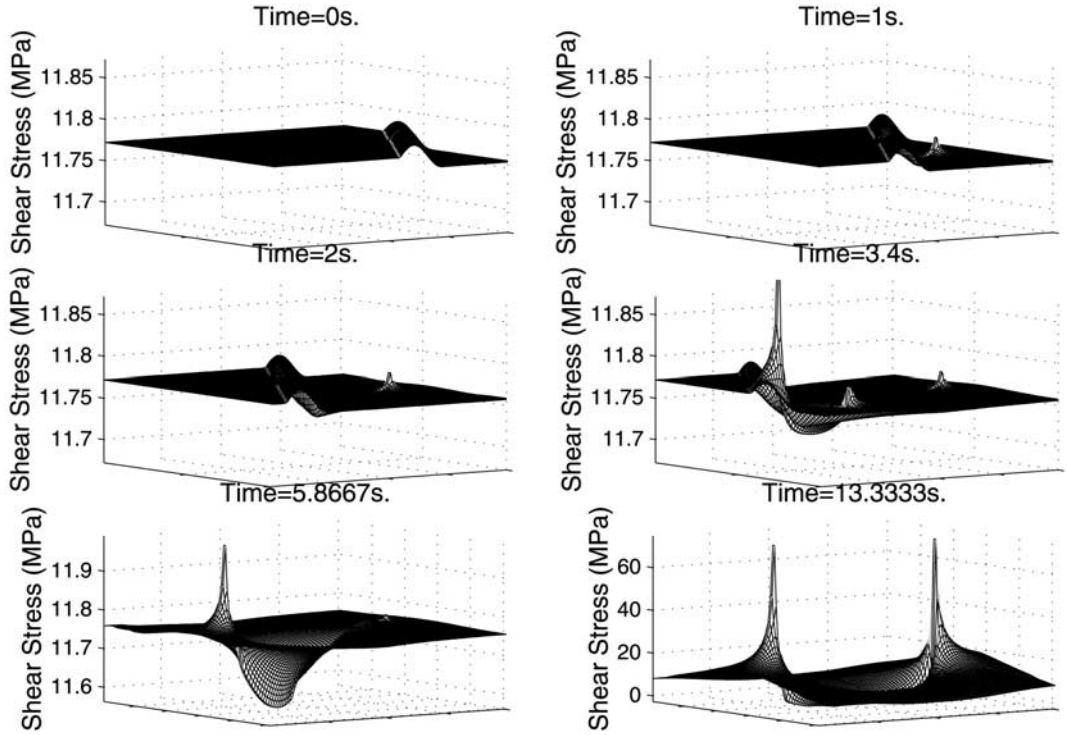

Figure 3. Space-time evolution of the stress field on and around the fault. The CFF is composed of a positive dynamic pulse followed by the negative static stress field. The fault has a length $L = 10$ km. The shear wave velocity is $c = 3000$ m/s, and the density of the medium is $\rho = 3000$ kg/m^3. The normal stress S_N is assumed to correspond to a depth of 5 km. A nonlinear friction law with varying weakening rate is considered on the fault.

on such a fault [*Voisin*, 2001, 2002]. For each value of D_c and for the three loadings, we measure the triggering delay between the loading and the eventual rupture. The positive stress pulse or a positive stress step both promote the nucleation of the impending rupture. When the positive loading is large enough, in terms of amplitude or duration, the fault describes the whole nucleation part and subsequently enters the unstable initiation phase. At this moment, nothing can stop the fault from evolving toward the rupture except for the negative dynamic pulse or a negative stress step. The occurrence of rupture depends on the balance between the loading parameters and the friction parameters. Figure 4 presents the results of this study. The triggering delay is increasing with the value of D_c independently from the loading. This is due to the decrease in the slope of friction with D_c: The characteristic time of friction is increasing. There is no clear difference in the triggering delay for $D_c < 0.5$ m. The differences appear when D_c is about 0.8 m. Above this value it is not possible to trigger faults with stress shadow loading, while it is still possible to trigger the same fault with the dynamic pulse and stress trigger loadings. When D_c is about 0.9 m, it becomes impossible to trigger the faults with the long-distance loading, too. The stress trigger loading only remains efficient. This experiment shows that triggering in stress shadows and at long distances, both related to the dynamic stress pulse, occurs on the most unstable faults and has a time-limited efficacy. The largest triggering delay expected for a dynamic loading or a stress shadow loading is related to the characteristic time associated with the value of D_c marked by the arrows in Figure 4. This relation cannot be stated in a simple expression since it depends on the shape of the friction law and on the shape of the loading.

4.2. Effect of the Frequency Content of the Dynamic Pulse

[21] For each friction law or equivalently for each value of D_c or β we first determine the limit frequency of the dynamic stress pulse that allows for triggering. Figure 5 presents the dependence of the limit frequency of triggering $f_{\lim}$ with β for three different cases. The blue squares mark the triggering threshold when the loading is formed by a dynamic stress pulse only. Pink squares mark the triggering threshold when the loading is formed by a dynamic stress pulse followed by a negative static stress field of equal amplitude. Finally, the red squares mark the triggering threshold when the loading is formed by the same dynamic stress pulse followed by a negative static stress field of amplitude 10 times larger than the maximum of the dynamic pulse. The three thresholds are different, confirming that the occurrence of triggering is due to the balance between the intrinsic mechanics of the fault and the external loading. Since the dynamic pulse is the same in the three cases, this result demonstrates that the whole CFF has to be considered in the triggering of seismicity. We observe that $f_{\lim}$ increases with β; that is to say, the triggering domain extends toward higher frequencies with increasing β. For a given value of β, $f_{\lim}$ decreases as the static stress field becomes more and

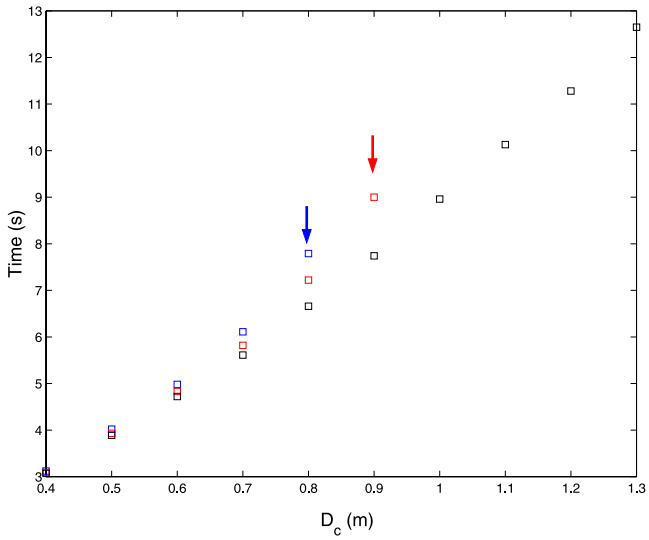

Figure 4. Triggering delay as a function of both the critical slip D_c (or, equivalently, β) and the loading. For each value of D_c ranging between 0.4 and 1.3 m, we performed three simulations with the three loadings presented in Figure 2. In the case of a stress shadow loading, it is impossible to trigger the fault with a D_c greater than 0.8 m. In the case of a long-distance loading, it is impossible to trigger a fault with a D_c greater than 0.9 m. On the contrary, in the case of a stress trigger loading, it is always possible to trigger the fault with any value of D_c. This result is consistent with the observation that dynamic triggering has a finite duration, while the static triggering has a wider effect on the regional seismicity after a major event.

more negative. The nucleation process is easily stopped by a large negative static stress field. The loading exerted by the dynamic stress pulse has to be larger to compensate for the larger static stress field. This can be achieved by either an increase in the amplitude of the pulse or by an increase in the duration of the loading, that is, a decrease of its frequency. A surprising effect of the negative static stress field is the deletion of the jump in the threshold curve as β tends to β_1. This also contributes to reducing the triggering domain to lower frequencies and is consistent with a seismicity rate decrease. Figure 5 also shows an interesting result: The same given frequency has a varying triggering potential, depending on whether or not there is a static stress field. To give an example, let us consider a frequency of 1 Hz. In the far field this frequency may trigger faults moderately unstable with β larger than 2.5. In a light stress shadow the same frequency may trigger faults with β larger than 2.8. In a heavy stress shadow zone it may trigger faults with β larger than 7, that is, faults that are highly unstable and are associated with a short characteristic time. Again, this is the illustration that we should consider the whole CFF in seismicity triggering studies.

4.3. Limitations Due to the Finite Difference Computations

[22] The computations presented in this article are achieved with the finite difference code described by *Ionescu and Campillo* [1999], adapted to the case of an external stress loading. Because of intrinsic limitations of the numerical scheme, we are not able to compute time evolution of the fault slip longer than a few minutes. However, it is not a theoretical limit of the triggering model that predicts a wide range of initiation duration, from a few seconds when β tends to infinity, to years or more when β tends to the stability limit β_0. Consequently, our working hypothesis is that the results presented in section 4.1 and in Figure 4 are representative of what happens on a timescale of a few days or weeks, even if we can describe only the timescale of a few seconds to a few minutes.

5. Comparison of the Numerical Results With Observed Data Sets

[23] In section 4 we presented numerical results about the possibility of triggering by dynamic and static triggering and also about the timing of triggering as a function of the loading. Now we intend to look at observed data to test the validity of the model. Although finite difference simulations are able to reproduce short time evolution (of the order of a few minutes), the theoretical model allows for short and long duration of nucleation and triggering delay. Consequently, we will try in the following to point out some characteristics of the triggering mechanisms through the analysis of the 1992 Landers and 1999 Hector Mine

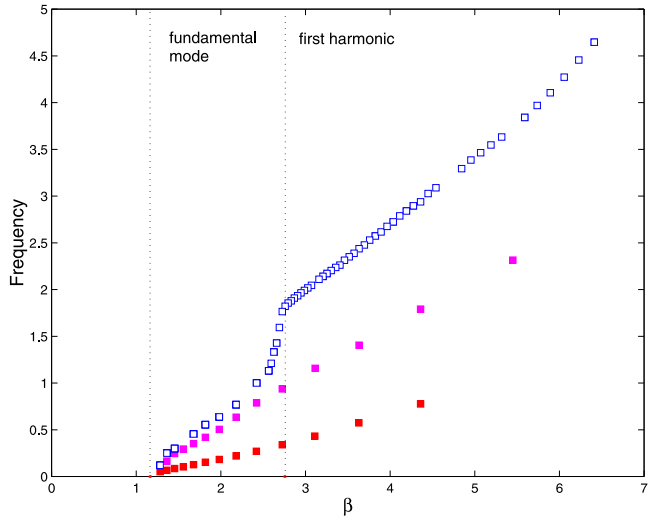

Figure 5. Triggering frequency limit $f_{\lim}$ with β. Blue squares represent the triggering limit due to a long-distance loading type. It is an extension of the previous results given by *Voisin* [2001]. Pink squares correspond to the triggering limit due to a stress shadow loading type. The negative static stress field has a unit amplitude. Note that the jump observed when β tends to β_1 with a long-distance loading type has been suppressed. This is a major effect of the negative static stress field. The triggering domain is now limited to lower frequencies. This is consistent with the seismicity rate decrease observed in actual stress shadows. Red squares correspond to the triggering limit due to a strong stress shadow loading type. The negative static stress field is 10 times larger than for the previous case. Note that the triggering limit is different: The larger the static stress field amplitude is, the lower the limit frequencies are.

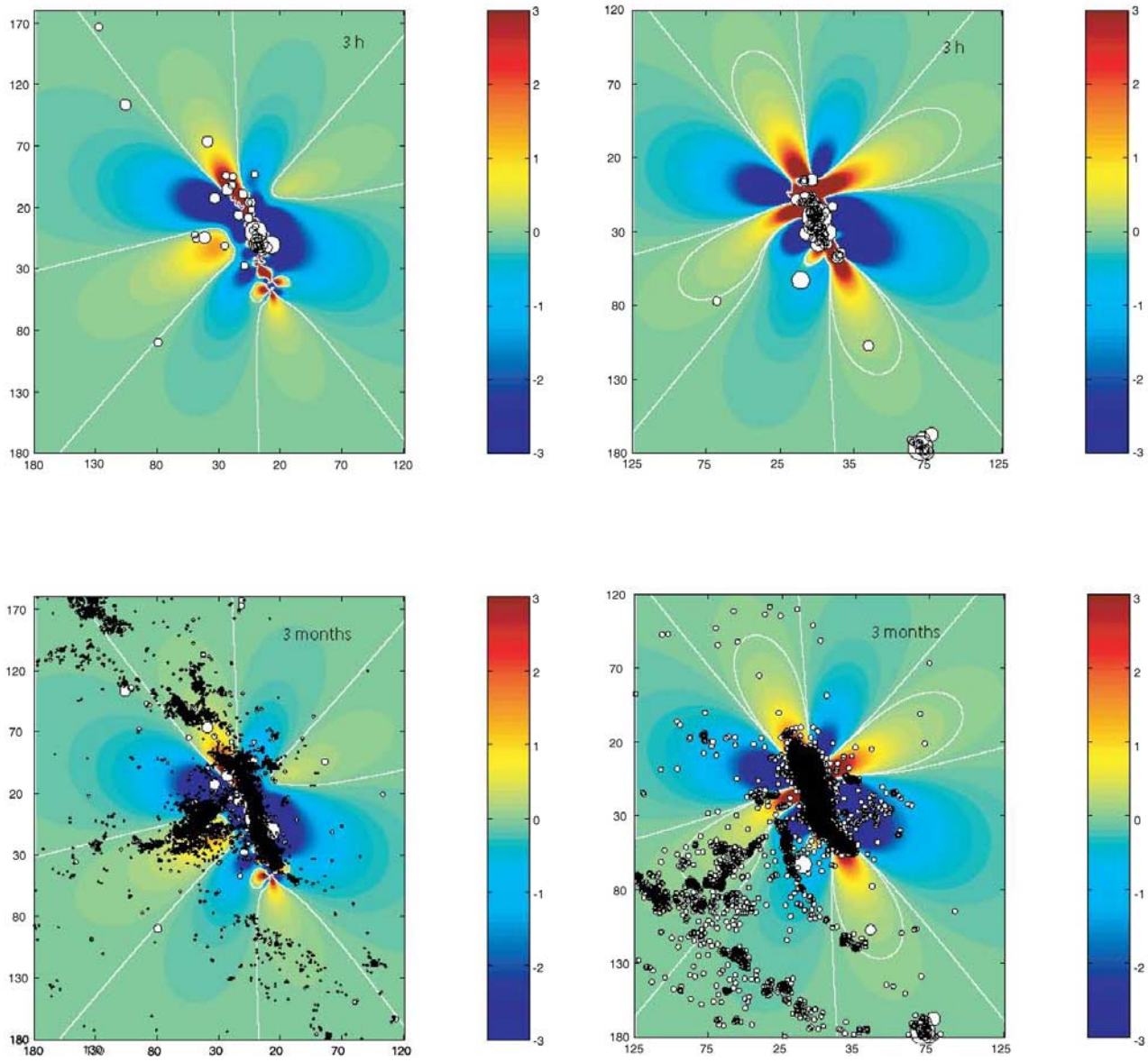

Figure 6. (top) First 3 hours of seismicity after the M_w 7.3 Landers earthquake and the M_w 7.1 Hector Mine earthquake against the respective Coulomb stress changes. The size of the circles representing the aftershocks is inversely proportional to the time elapsed between the main rupture and each aftershock occurrence. Concerning the Landers earthquake, the first aftershocks recorded occur indifferently in the stress trigger zones, in the stress shadow zones, or at long distances. For the Hector Mine earthquake the first aftershock recorded by the seismic network occurred around the Salton Sea, about 150 km away from the epicenter. (bottom) First 3 months of seismicity after the M_w 7.3 Landers earthquake and the M_w 7.1 Hector Mine earthquake against the respective Coulomb stress changes. The classical pattern of aftershock distribution is clearly visible for the Landers earthquake, much less for the Hector Mine earthquake.

aftershock sequences. The intent is less to check the validity of the model than either to confirm or to deny the consistency of the model with observed data.

5.1. Triggering of Aftershocks on a Short Timescale of 3 Hours

[24] Figure 6 (top) plots the first 3 hours of seismicity after the M_w 7.3 Landers earthquake and the M_w 7.1 Hector Mine earthquake against the respective Coulomb stress changes. The Coulomb stress changes are computed at a depth of 4.5 km, on the optimally oriented planes, considering the regional stress field. The Coulomb 2.1 code was used [*Toda et al.*, 1998]. The size of the circles representing the aftershocks is inversely proportional to the time elapsed between the main rupture and each aftershock occurrence. This unusual representation shows that the early aftershocks occur either at remote distances, in the stress shadow zones, or in the stress trigger zones indifferently. The first after-

shock recorded after the 1992 Landers earthquake occurred along the fault trace. Actually, most aftershocks occur along the fault trace or in stress shadows, except for the future Big Bear earthquake. Concerning the Hector Mine earthquake, the first aftershock recorded occurred south of the rupture, in the rupture direction, near Salton Sea nearly 180 km away from the main shock. In this region the seismicity immediately increased at the passage of the waves emitted by the main shock [*Gomberg et al.*, 2001]. More than 50 events occurred in a few days, the first of them 59 s after the main shock. It appears that the fault system around the Salton Sea was quite unstable as testified by the slow accelerating curve of cumulative number of events [*Gomberg et al.*, 2001]. The same phenomenon was observed 250 km south from the epicenter, in the Mexicali Valley (Baja California, Mexico), at exactly the same azimuth [*Glowacka et al.*, 2002]. The main difficulty in this analysis is the incompleteness of the aftershock catalogues. This is particularly true for the Landers earthquake, for which stations were added in the few hours after the rupture. However, there is no reason that we should miss more aftershocks in the stress trigger than in the stress shadow zones. Consequently, despite the data scarcity, the results are meaningful and show that aftershocks occur indifferently in stress shadows, in stress triggers, or at large distances. The major faults seem to be insensitive to the main shock on such a short timescale: No aftershock activity is recorded along the San Andreas or the San Jacinto fault.

[25] We use the β statistic method [*Matthews and Reasenberg*, 1988] to demonstrate the reality of triggering of these aftershocks shown in Figure 6. Note that β has a different meaning here than in section 4. However, in order to keep on with notations used in previous studies, we have decided to give the same name to the β statistics and to the nondimensional weakening parameter. The β statistic simply compares the number of aftershocks before and after the main shock in any given region. Despite the small number of earthquakes recorded during the first 3 hours, and the bias it may produce [*Marsan*, 2003], we decided to create β maps associated with the 1992 Landers and the 1999 Hector Mine earthquakes. The smoothed β statistic is sensitive to a contrast of average seismicity rate between two time intervals [*Matthews and Reasenberg*, 1988; *Gomberg et al.*, 2001]. Rate changes are calculated for a 3-hour and 3-month period immediately after each main shock, relative to the 3 months before each event (background period). Figure 7 (left) shows the β statistic map for the first 3 hours after the Landers and Hector Mine earthquakes. The β maps on a timescale of 3 hours clearly exhibit the directivity of each rupture: north for the Landers earthquake and south for the Hector Mine earthquake. Large values of β indicate a triggered seismicity. The comparison between the Coulomb stress maps and the β maps demonstrates that the seismicity recorded a few hours after each rupture is triggered by each main shock.

5.2. Triggering of Aftershocks on a Timescale of 3 Months

[26] Figure 6 (bottom) plots three months of seismicity after the Landers and Hector Mine earthquakes with the same representation: The size of the circles scales inversely with the time elapsed since the main shock. The classical spatial pattern of aftershocks between stress triggers and stress shadows is clearly visible for the 1992 Landers earthquake, much less so for Hector Mine. An interesting feature of the 1999 Hector Mine aftershock sequence lies in the appearance of triggered seismicity on NW-SE faults later in time. These faults and lineaments are parallel to the San Andreas Fault system and parallel to the faults that experienced triggered stable slip [*Sandwell et al.*, 2000]. Aftershocks begin to appear on these faults a few weeks after the main shock. The response of these major structures is delayed by 2 months and develops simultaneously with the swarms of aftershocks. We will show that such a long time delay is compatible with the effect of the static stress change. Figure 7 (right) shows the corresponding β statistic maps. They look pretty similar. The major structures like the San Andreas fault zone (SAFZ) or the San Jacinto fault zone exhibit triggered seismicity (testified by large values of β) that were not present on a timescale of 3 hours. The directivity of the major rupture, which was readable on a timescale of 3 hours, is not visible anymore. This is also consistent with a static stress change that does not exhibit any directivity.

5.3. Seismicity of the Salton Sea Area

[27] The seismicity around the Salton Sea is extremely interesting. The Landers earthquake, with a directivity to the north, did not trigger any event in this region on the short timescale of 3 hours. However, the Hector Mine earthquake, with directivity to the south, triggered a collection of events [*Gomberg et al.*, 2001] on a short timescale of a few minutes. If we focus now on the longer timescale of 3 months, we see that the Salton Sea region is active for both the Landers and Hector Mine earthquakes. This suggests that the Salton Sea faults are highly unstable and can be triggered by both dynamic stress waves on a short timescale and static stress change on a longer timescale. At such a distance from the main shocks (about 150 km) the static stress change is much less than 0.01 bars. However, according to *Ziv and Rubin* [2000] this can be sufficient to trigger the seismicity. If this is the triggering factor, it implies that the same region can be activated indifferently by dynamic and/or static stress changes. This would also imply that the triggering mechanisms are the same for dynamic and static triggering.

6. Discussion

6.1. Friction Properties and Triggering Potential of the Different Loadings

[28] A fault as a geological object interacts with its environment and with other faults. Dynamic and static stress changes affect the fault evolution: High amplitudes of stress waves and/or long duration of the static stress increase both favor the stability/instability transition and hasten the triggering of the impending event. The slip-dependent friction model with a stability/instability transition was used to study the 1980 Irpinia (Italy) earthquake, formed of three subevents successively triggered every 20 s [*Voisin et al.*, 2000]. Fault geometry and time delay were known; we inverted for the possible values of β that lead to the observed 20-s delay as a function of the loading. The results are summarized in Figure 8. We have now extended the

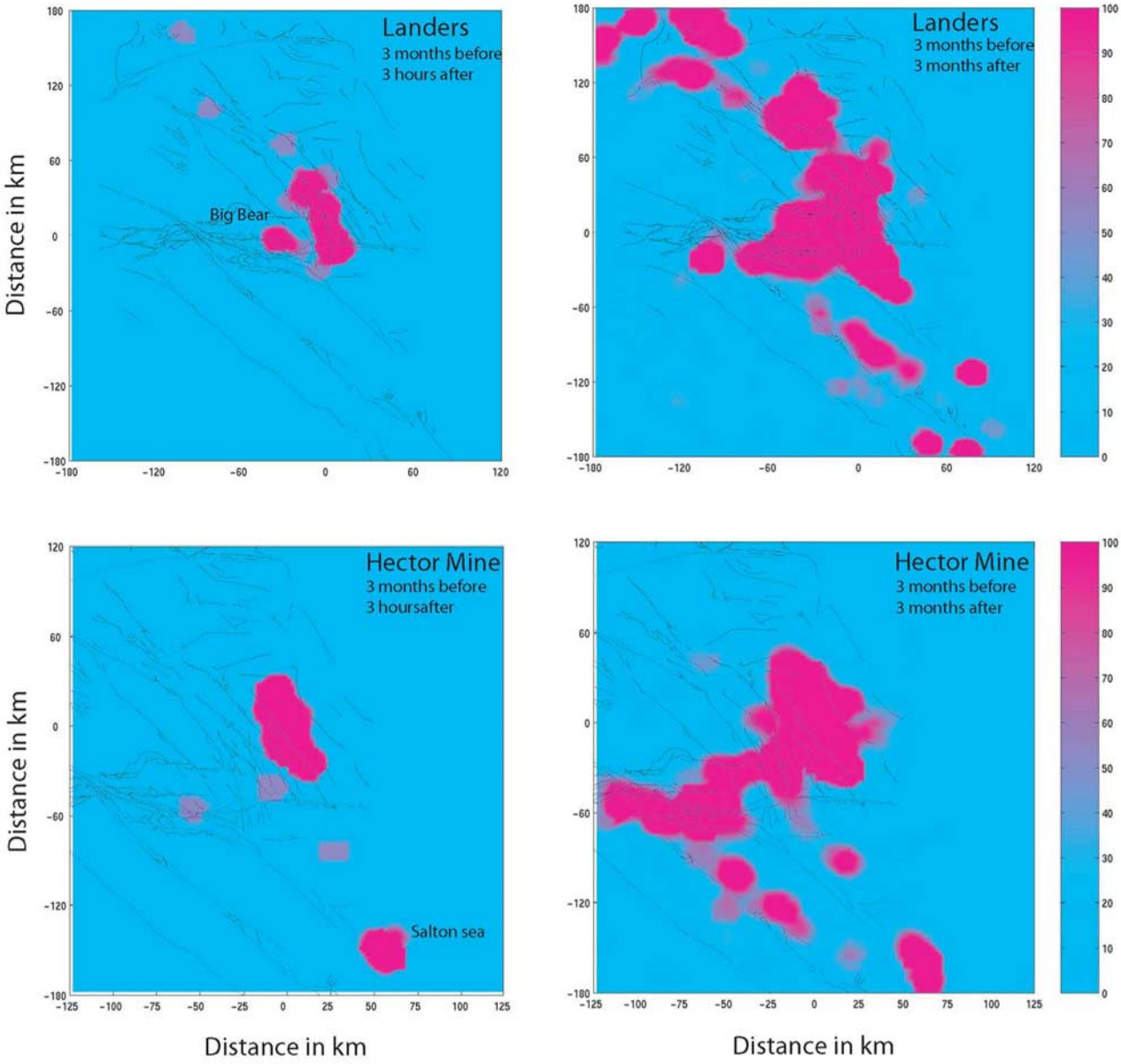

Figure 7. (left) First 3 hours smoothed β statistic maps after the Landers and Hector Mine earthquakes. Smoothed β statistic is sensitive to a contrast of average seismicity rate between two time intervals [*Matthews and Reasenberg*, 1988; *Gomberg et al.*, 2001]. Rate change is calculated for a 3-hour period immediately after each main shock, relative to the 3 months before each event (background period). Areas with β statistic >50.0 are suggestive of a significant average rate increase. (right) First 3 months smoothed β statistic maps after the Landers and Hector Mine earthquakes. Rate change is relative to the 3 months before each event.

simulations and have added the new computations for antishock triggering as presented in section 3 (line 3). Under a dynamic plus static loading (line 1), the suitable values for β correspond to either stable or unstable faults. Under a dynamic loading only (line 2), the faults that will experience a triggering delay of 20 s are more unstable. Finally, under a dynamic minus static loading (line 3), the faults have to be very unstable to lead to a 20-s delay. In other words, for a given time delay (here 20 s), the loading picks out different faults with wide differences in their stability/instability properties.

[29] Figure 8 also describes the domain of action of the different loadings. A dynamic plus static loading (stress trigger loading) can trigger every fault, even the most stable associated with a large characteristic time. This could explain long time interaction, as described for Southern Californian earthquake sequences or for the North Anatolian earthquake sequence [*Stein et al.*, 1997]. A dynamic loading alone (long-distance loading) can trigger only a fraction of the faults: those that are unstable or weakly stable (depending on the amplitude of the stress waves). This implies that dynamic triggering is efficient on

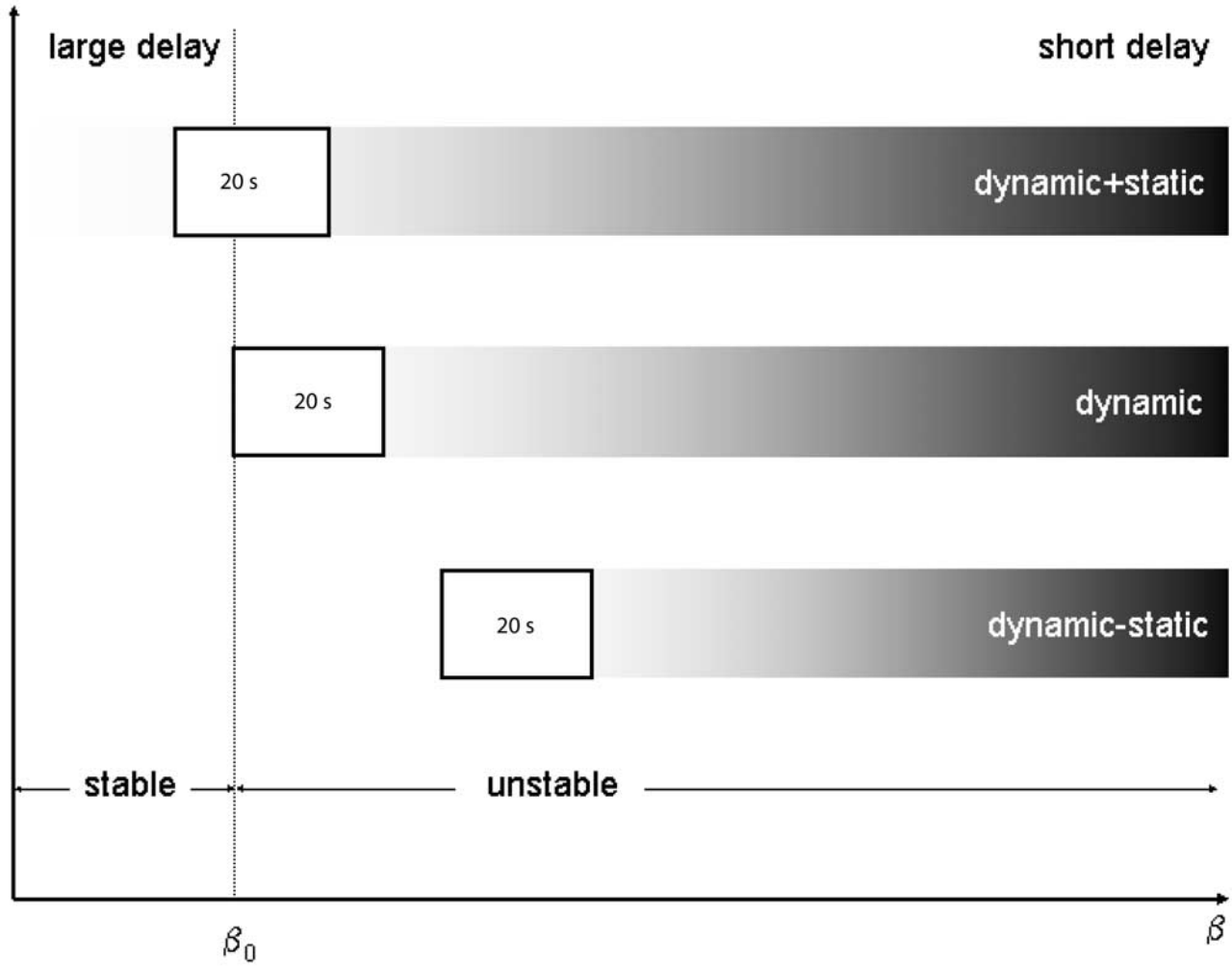

Figure 8. β values that lead to a 20-s delay as a function of the loading. Under a dynamic plus static loading (line 1), the suitable values for β correspond to either stable or unstable faults. Under a dynamic loading only (line 2), the faults that will experience a triggering delay of 20 s are more unstable. Finally, under a dynamic minus static loading (line 3), the faults have to be very unstable to lead to a 20-s delay.

a much shorter timescale than static triggering. However, this finite duration of dynamic triggering may be much longer than the wave's duration. Finally, a dynamic minus static loading (stress shadow loading) triggers only the most unstable faults, associated with a small characteristic time. This may explain the apparent burst of antishocks in the first hours following the Landers and Hector Mine earthquakes.

6.2. Fault Maturity and Triggering Potential of the Different Loadings

[30] Variations in time delay between stress loading and fault response are related to fault frictional properties and therefore to the critical slip D_c. Laboratory experiments show that D_c, generally interpreted in terms of the mechanics of contact junctions on fresh surfaces, also depends on gouge thickness. Indeed, there is a clear relationship between gouge thickness and cumulative fault slip (the fault thickens as the slip accumulates) and consequently between cumulative slip and D_c. Faults with a large cumulative slip and a large D_c will be considered as mature faults. As an example, the San Andreas fault, with its long history and well-developed gouge, is a mature system [*Marone and Kilgore*, 1993]. On the other hand, faults located in eastern California and western Nevada where numerous earthquakes are recorded are immature (shorter length and small cumulative slip). Mature faults are associated with larger D_c, and their stability is then greater than that of immature faults (Figure 1). The question of stability/instability is related to β. Coming back to its definition, β is the product of the weakening rate release by a characteristic length L. In case of a single homogeneous fault, L would stand for the length of the fault. In case of a heterogeneous fault, L could stand for the length of the fault, or any shorter characteristic length, typical of the roughness of the fault surfaces or of its width. The stability condition must be given relative to a size. The SAFZ can be at the same time stable at the overall scale and unstable at the local scale. Previous studies by *Campillo et al.* [2001] and *Voisin et al.* [2002] have shown that heterogeneity is a stabilizing factor. The more complex a fault system is, the more stable it can be. According to our model, faults respond quietly and slowly to a stress pertur-

bation because of a longer characteristic time. An immediate consequence is the insensitivity of these mature faults to the dynamic stress perturbations, as observed on our 3-hour β maps (Figure 7), at Parkfield after the 1992 Landers earthquake [*Gomberg and Bodin*, 1994] or after the 1999 Hector Mine earthquake.

[31] The stability/instability model implies that dynamic and static stress triggering pertain to the same physical process; only their timescales of efficacy are different. The delay before the triggering depends on β, which represents the intrinsic fault friction properties, and on the complete loading history.

[32] The triggering threshold is double: First, the stress on the fault must equal the static friction μ_s. Then the loading must ensure that the fault enters the unstable part of its friction law. This is guaranteed with large amplitude and/or long duration of the loading. For a mature fault system, because of a larger characteristic slip D_c the second threshold of slip is out of reach of the dynamic stress waves, while a static stress step promotes the creep on such a fault or a possible triggering with a long time delay.

6.3. Implications for Seismic Hazard

[33] This model, if correct, has profound implications for seismic hazard analysis: Stress changes do influence the occurrence of small and large shocks differently. Large shocks are restricted to large faults which have accumulated a large amount of cumulative slip and can be considered as mature.

[34] The model that we present here predicts that those faults are insensitive to any stress changes but static. However, the model does not predict any given magnitude for the earthquake triggered by the static change. This magnitude is dependent on the state of stress of the fault and possibly on the state of the fault surface when considering rate and state friction. In other words, a large mature fault can experience both large and small earthquakes. Our model simply predicts that static stress changes are able to initiate seismicity on the large and mature faults, while dynamic stress changes are not.

7. Conclusions

[35] We propose a model based on a slip-dependent friction law that encompasses in a single framework static and dynamic triggering of seismicity, triggering of antishocks in stress shadows, and the possibility of creep events. The time delay between the loading and the triggering is related to the balance between the shape of the loading and the friction parameters. Consequently, it is essential to consider complete Coulomb failure functions that include static and dynamic loadings to understand seismicity triggering.

[36] The finite duration of dynamic triggering and the large duration of static triggering are explained by the model. However, the model does not constrain the range of actual dynamic triggering delays.

[37] The model seems to be consistent with actual data: At short timescales, indifferent triggering in stress triggers, in stress shadows, and at remote distances is explained by a dynamic effect. At larger timescales, triggering of seismicity on large mature fault systems is explained by a static effect on mature faults, with larger D_c and larger characteristic time.

[38] **Acknowledgments.** The authors would like to thank R. Harris, M. E. Belardinelli, and an anonymous reviewer for their thorough reviews. We thank M. Campillo, J. Gomberg, I. Ionescu, and D. Marsan for meaningful discussions and/or reviews. J. Gomberg and P. A. Reasenberg are acknowledged for providing their β statistic codes. Earthquake data were retrieved from the SCEC. Computations were achieved at LGIT with technical support from C. Péquegnat and G. Escorne. This paper benefited from financial support by ACI "Risques Naturels et Changements Climatiques." C.V. dedicates this paper to Jacqueline Lamouroux-Defarcy (1928–2003).

References

Anderson, J. G., J. N. Brune, J. N. Louie, Y. Zeng, M. Savage, G. Yu, Q. Chen, and D. dePolo (1994), Seismicity in the western Great Basin apparently triggerd by the Landers, California, earthquake, 28 June 1992, *Bull. Seismol. Soc. Am.*, *84*, 863–891.

Antonioli, M., M. Cocco, S. Das, and C. Henry (2003), Dynamic stress triggering during the great 25 March 1998 Antarctic Plate earthquake, *Bull. Seismol. Soc. Am.*, *92*, 896–903.

Belardinelli, M. E., M. Cocco, O. Coutant, and F. Cotton (1999), Redistribution of dynamic stress during coseismic ruptures: Evidence for fault interaction and earthquake triggering, *J. Geophys. Res.*, *104*, 14,925–14,945.

Belardinelli, M. E., A. Bizzarri, and M. Cocco (2003), Earthquake triggering by static and dynamic stress changes, *J. Geophys. Res.*, *108*(B3), 2135, doi:10.1029/2002JB001779.

Bodin, P., and J. Gomberg (1994), Triggered seismicity and deformation between the Landers, California, and Little Skull Mountain, Nevada, earthquakes, *Bull. Seismol. Soc. Am.*, *84*, 835–843.

Brodsky, E., V. Karakostas, and H. Kanamori (2000), A new observation of dynamically triggered regional seismicity: Earthquakes in Greece following the August, 1999 Izmit, Turkey earthquake, *Geophys. Res. Lett.*, *27*, 2741–2744.

Campillo, M., and I. R. Ionescu (1997), Initiation of antiplane shear instability under slip-dependent friction, *J. Geophys. Res.*, *102*, 20,363–20,371.

Campillo, M., I. R. Ionescu, P. Favreau, and C. Voisin (2001), On the effective friction law of a heterogeneous fault, *J. Geophys. Res.*, *106*, 16,307–16,322.

Cotton, F., and O. Coutant (1997), Dynamic stress variations due to shear faults in a plane layered medium, *Geophys. J. R. Astron. Soc.*, *50*, 643–668.

Das, S., and C. H. Scholz (1981), Off-fault aftershock clusters caused by shear stress increase?, *Bull. Seismol. Soc. Am.*, *71*, 1669–1675.

Dascalu, C., I. R. Ionescu, and M. Campillo (2000), Fault finiteness and initiation of dynamic shear instability, *Earth Planet. Sci. Lett.*, *177*, 163–176.

Glowacka, E., F. A. Nava, G. D. de Cossio, V. Wong, and F. Farfan (2002), Fault slip, seismicity, and deformation in Mexicali Valley, Baja California, Mexico, after the *M* 7.1 1999 Hector Mine earthquake, *Bull. Seismol. Soc. Am.*, *92*, 1290–1299.

Gomberg, J., and P. Bodin (1994), Triggering of the M_s = 5.4 Little Skull Mountain, Nevada, earthquake with dynamic strain, *Bull. Seismol. Soc. Am.*, *84*, 844–853.

Gomberg, J., M. L. Blanpied, and N. M. Beeler (1997), Transient triggering of near and distant earthquakes, *Bull. Seismol. Soc. Am.*, *87*, 294–309.

Gomberg, J., N. M. Beeler, M. L. Blanpied, and P. Bodin (1998), Earthquake triggering by transient and static deformations, *J. Geophys. Res.*, *103*, 24,411–24,426.

Gomberg, J., P. A. Reasenberg, P. Bodin, and R. A. Harris (2001), Earthquake triggering by seismic waves following the Landers and Hector Mine earthquakes, *Nature*, *411*, 462–466.

Gomberg, J., P. Bodin, and P. A. Reasenberg (2003), Observing earthquakes triggered in the near-field by dynamic deformations, *Bull. Seismol. Soc. Am.*, *93*, 118–138.

Hamilton, R. B. (1972), Aftershocks of the Borrego Mountain earthquake from April 12 to June 12, 1968, in *The Borrego Mountain Earthquake of April 9, 1968*, *Geol. Surv. Prof. Pap. 787*, pp. 31–54, U.S. Govt. Print. Off., Washington, D. C.

Harris, R. A. (1998), Introduction to special section: Stress triggers, stress shadows, and implications for seismic hazard, *J. Geophys. Res.*, *103*, 24,347–24,358.

Harris, R. A., and S. M. Day (1993), Dynamics of fault interaction: Parallel strike slip faults, *J. Geophys. Res.*, *98*, 4461–4472.

Harris, R. A., and R. W. Simpson (1996), In the shadow of 1857: The effect of the great Ft. Tejon earthquake on subsequent earthquakes in southern California, *Geophys. Res. Lett.*, *23*, 229–232.

Harris, R. A., and R. W. Simpson (1998), Suppression of large earthquakes by stress shadows: A comparison of Coulomb and rate-and-state failure, *J. Geophys. Res.*, *103*, 24,439–24,451.

Harris, R. A., R. J. Archuleta, and S. M. Day (1991), Fault steps and the dynamic rupture process: 2D numerical simulations of a spontaneously propagating shear fracture, *Geophys. Res. Lett.*, *18*, 893–896.

Hill, D. P., P. A. Reasenberg, A. Michael, W. J. Arabaz, and G. C. Beroza (1993), Seismicity remotely triggered by the magnitude 7.3 Landers, California, earthquake, *Science*, *260*, 1617–1623.

Ionescu, I. R., and M. Campillo (1999), Influence of the shape of friction law and fault finiteness on the duration of initiation, *J. Geophys. Res.*, *104*, 3013–3024.

Kadinski-Cade, K., and R. J. Willemann (1982), Towards understanding aftershock patterns: The basic pattern for strike-slip earthquakes, *Eos Trans. AGU*, *63*, 384.

Kame, N., and T. Yamashita (1987), Dynamic nucleation process of shallow earthquake faulting in a fault zone, *Geophys. J. Int.*, *128*, 204–216.

Kase, Y., and K. Kuge (1998), Numerical simulation of spontaneous rupture processes on two non-coplanar faults: The effect of geometry on fault interaction, *Geophys. J. Int.*, *135*, 911–922.

Kase, Y., and K. Kuge (2001), Rupture propagation beyond fault discontinuities: Significance of fault strike and location, *Geophys. J. Int.*, *147*, 330–342.

Kilb, D. (2003), A strong correlation between induced peak dynamic Coulomb stress change from the 1992 *M* 7.3 Landers, California, earthquake and the hypocenter of the 1999 *M* 7.1 Hector Mine, California, earthquake, *J. Geophys. Res.*, *108*(B1), 2012, doi:10.1029/2001JB000678.

Kilb, D., J. Gomberg, and P. Bodin (2000), Earthquake triggering by dynamic stresses, *Nature*, *408*, 570–574.

Kilb, D., J. Gomberg, and P. Bodin (2002), Aftershock triggering by complete Coulomb stress changes, *J. Geophys. Res.*, *107*(B4), 2060, doi:10.1029/2001JB000202.

Marone, C., and B. Kilgore (1993), Scaling of the critical slip distance for seismic faulting with shear strain in fault zones, *Nature*, *362*, 618–621.

Marone, C. (2000), Shaking faults loose, *Nature*, *408*, 533–534.

Marsan, D. (2003), Triggering of seismicity at short timescales following Californian earthquakes, *J. Geophys. Res.*, *108*(B5), 2266, doi:10.1029/2002JB001946.

Matthews, M. V., and P. A. Reasenberg (1988), Statistical methods for investigating quiescence and other temporal seismicity patterns, *Pure Appl. Geophys.*, *126*, 357–372.

Ohnaka, M. (1996), Non uniformity of the constitutive law parameters for shear rupture and quasistatic nucleation to dynamic rupture: A physical model of earthquake generation process, *Proc. Natl. Acad. Sci. U. S. A.*, *93*, 3795–3802.

Parsons, T., R. S. Stein, R. W. Simpson, and P. A. Reasenberg (1999), Stress sensitivity of fault seismicity: A comparison between limited-offset oblique and major strike-slip faults, *J. Geophys. Res.*, *104*, 20,183–20,202.

Perfettini, H., J. Schmittbuhl, and A. Cochard (2003a), Shear and normal load perturbations on a two-dimensional continuous fault: 1. Static triggering, *J. Geophys. Res.*, *108*(B9), 2408, doi:10.1029/2002JB001804.

Perfettini, H., J. Schmittbuhl, and A. Cochard (2003b), Shear and normal load perturbations on a two-dimensional continuous fault: 2. Dynamic triggering, *J. Geophys. Res.*, *108*(B9), 2409, doi:10.1029/2002JB001805.

Reasenberg, P. A., and R. W. Simpson (1992), Response of regional seismicity to the static stress change produced by the Loma Prieta earthquake, *Science*, *255*, 1687–1690.

Rybicki, K. (1973), Analysis of aftershocks on the basis of dislocation theory, *Phys. Earth Planet. Inter.*, *7*, 409–422.

Sandwell, D. T., L. Sichoix, D. Agnew, Y. Bock, and J. B. Minster (2000), Near real-time radar interferometry of the Mw 7.1 Hector Mine earthquake, *Geophys. Res. Lett.*, *27*, 3101–3104.

Simpson, R. W., and P. A. Reasenberg (1994), Earthquake-induced static stress changes on central California faults, in *The Loma Prieta, California, Earthquake of October 17, 1989, Part F: Tectonic Processes and Models*, *U.S. Geol. Surv. Prof. Pap. 1550-F*, edited by R. W. Simpson, U.S. Geol. Surv., Denver, Colo.

Smith, S. W., and W. Van de Lindt (1969), Strain adjustments associated with earthquakes in southern California, *Bull. Seismol. Soc. Am.*, *59*, 1569–1589.

Stein, R. S. (1999), The role of stress transfer in earthquake occurrence, *Nature*, *402*, 605–609.

Stein, R. S., and M. Lisowski (1983), The 1979 Homestead Valley earthquake sequence, California: Control of aftershocks and postseismic deformation, *J. Geophys. Res.*, *88*, 6477–6490.

Stein, R. S., A. A. Barka, and J. H. Dieterich (1997), Progressive failure on the North Anatolian fault since 1939 by earthquake stress triggering, *Geophys. J. Int.*, *128*, 594–604.

Toda, S., R. S. Stein, P. A. Reasenberg, J. H. Dieterich, and A. Yoshida (1998), Stress transferred by the 1995 M_w = 6.9 Kobe, Japan, shock: Effect on aftershocks and future earthquake probabilities, *J. Geophys. Res.*, *103*, 24,543–24,565.

Voisin, C. (2001), Dynamic triggering of earthquakes: The linear slip-dependent friction case, *Geophys. Res. Lett.*, *28*, 3357–3360.

Voisin, C. (2002), Dynamic triggering of earthquakes: The nonlinear slip-dependent friction case, *J. Geophys. Res.*, *107*(B12), 2356, doi:10.1029/2001JB001121.

Voisin, C., M. Campillo, I. Ionescu, F. Cotton, and O. Scotti (2000), Dynamic versus static stress triggering and friction parameters: Inferences from the November 23, 1980, Irpinia earthquake, *J. Geophys. Res.*, *105*, 21,647–21,659.

Voisin, C., I. R. Ionescu, M. Campillo, R. Hassani, and Q. L. Nguyen (2002), Process and signature of initiation on a finite fault system: A spectral approach, *Geophys. J. Int.*, *148*, 120–131.

Yamashina, K. (1978), Induced earthquakes in the Izu Peninsula by the Izu-Hanto-Oki earthquake of 1974, Japan, *Tectonophysics*, *51*, 139–154.

Ziv, A., and A. M. Rubin (2000), Static stress transfer and earthquake triggering: No lower threshold in sight?, *J. Geophys. Res.*, *100*, 13,631–13,642.

F. Cotton, S. Di Carli, and C. Voisin, Laboratoire de Géophysique Interne et Tectonophysique, Observatoire des Sciences de l'Univers de Grenoble, Université Joseph Fourier, BP 53, F-38041 Grenoble, France. (fcotton@obs.ujf-grenoble.fr; sdicarli@obs.ujf-grenoble.fr; cvoisin@obs.ujf-grenoble.fr)